Available online at www.sciencedirect.com

ScienceDirect

Procedia Computer Science 232 (2024) 201–210

Procedia Computer Science

www.elsevier.com/locate/procedia

5th International Conference on Industry 4.0 and Smart Manufacturing

Hybrid prognosis of drill-bits based on direct inspection

Luca Bernini[a,b,*], Ugo Malguzzi[b], Paolo Albertelli[a,b], Michele Monno[a,b]

[a]*Department of Mechanical Engineering, Politecnico di Milano, Via La Masa, 1, Milan, 20156, Lombardy, Italy.*
[b]*MUSP, Macchine Utensili Sistemi di Produzione, strada della Torre della Razza, Piacenza, 29122, Emilia-Romagna, Italy.*

Abstract

Within the paradigm of industry 5.0, manufacturing systems are seeking for human-centred production, where the operator finds high-level supervision tasks. In this context, low-level decision making should be performed by machines themselves. In this paper, a hybrid prognosis algorithm is developed to automatically inspect the cutting edges of drill-bits and to predict their Remaining Useful Life (RUL) and the associated probability density function. The solution relies on the automatic measurement of flank wear through convolutional filtering and edge detection. Prognosis exploits particle filter, which updates multi-layer perceptron with online data, to adaptively predict drill-bits RUL. The solution reduces the experimental preliminary run-to-failures needed for training standard machine learning algorithms, exploiting them in a real-time adaptive scenario, while predicting tool RUL under untested and variable cutting process operations. The algorithm uses direct wear observations, taken during set-up times (e.g., tool changes, workpiece change), thus not interfering with the process.

Keywords: Hybrid prognostics; Direct drill-bit inspection; Image processing; Remaining Useful Life prediction.

1. Introduction

The new paradigm of Industry 5.0 added to Industry 4.0 societal goals as an objective for industry and production systems, only reachable through human-centric production processes [1]. Within this scenario, the operator tasks must reflect his new position. Thus, low-level decision making should be performed through machine intelligence, while high-level supervision and decision-making should be assigned to the machine operator. Consequently, monitoring

* Corresponding author.
E-mail address: luca1.bernini@polimi.it

1877-0509
10.1016/j.procs.2024.01.020

the manufacturing process and supporting maintenance decision-making become useful means to reach this goal.

Cutting tools monitoring and prognosis is an active research topic in the manufacturing field, due to cutting tools high impact on machine downtimes [2], production system economy [3] and rare materials usage [4]. Nevertheless, effective monitoring and prognosis solutions are far from being widely and robustly applied in industry. Indirect inspection and monitoring makes use of process measurements, like vibrations [5]–[7], cutting forces [5]–[9] and cutting power [10] to estimate the cutting tool condition in real-time. Signal features (e.g. mean, standard deviation, harmonic amplitudes and ranges, wavelet decompositions, etc.) [11], are generally passed to statistical-based and data-driven models to estimate whether the cutting tool has failed or not. Nevertheless, the above features are influenced by process parameters [8], like feed and spindle speed for a drilling application, while statistical-based algorithms (e.g., Auto-Regressive Moving-Average models) or data-driven models (e.g., Artificial Neural Networks) need a high quantity and quality of data to properly work [12]. The combination of these two characteristics makes state-of-art solutions not suitable for industrial applications. This is especially true for one-of-a-kind or small batch production, where cutting is performed under varying cutting conditions, where system retraining is needed and only limited training data are available [8]. On the other side, direct inspection makes use of point wise scanning, profilometric acquisitions [13] or 2D/3D calibrated pictures analysis [14] to evaluate the flank wear of the tool. However, these techniques are available only when the cutting tool is not processing the workpiece.

Both the inspection strategies can be used to feed prognosis algorithms with the goal of estimating the Remaining Useful Life (RUL) of cutting tools. State-of-art prognosis techniques can be categorized in four groups: model-based, statistical-based, data-driven and experience-based algorithms [12]. Despite these solutions are valuable for mass production, where high quantity of data are available for a limited pool of products, the need for a high number of run-to-failures (RTFs) and process parameter combinations is not affordable for small batch production realities.

In this paper, a hybrid solution is proposed, that fuses multiple algorithm categories, i.e., data-driven and statistical approaches, in order to forecast drill-bits wear starting from tool pictures. The solution adapts to different cutting parameters and unseen degradation trends, by leveraging on particle filter (PF) capability to adapt multi-layer perceptron (MLP) architectures (demonstrated in different domains, i.e. structural health monitoring [15] and batteries prognosis [16]). The solution needs a single training RTF to predict new drill-bits RUL and RUL probability density function (PDF). The predictions are updated as long as new drill-bit pictures come from the field. The conceived approach features generalisability (i.e., the MLP is a universal fitter and can adapt to different degradation trends) and scalability (i.e., MLPs can be deepened, widened, or substituted with other architectures, including even other inputs).

The structure of the paper is as follows: in section 2, the inspection phase is presented; then, direct drill-bit prognosis, through the hybridization of MLP and PF, is detailed, followed by the experimental campaign description., Results are discussed in section 3, followed by conclusions (section 4).

2. Materials and methods

In this section, the conceived solution is described in all its parts. The structure of the developed approach is schematized in Fig. 1. The conceived solution is based on a two layer architecture: an inspection layer processes drill-bits' cutting edges pictures to extract measurements of their flank wear; a prognosis layer, forecasts the evolution of drill-bit flank wear, starting from a limited knowledge of degradation trends and adapting to the unseen degradation trend when new pictures are available (Fig. 1). These layers will be explained in detail in the following subsections.

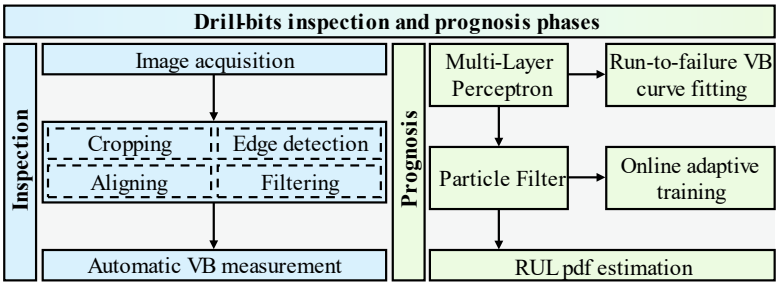

Fig. 1. Schematization of the conceived methodology.

Nomenclature

APE	Absolute prediction error
MLP	Multi-Layer Perceptron
MRR	Material Removal Rate
PDF	Probability density function
PF	Particle filter
PH	Prognostics horizon
RTF	Run-to-failure
RUL	Remaining Useful Life
α	Maximum allowable error
β	Minimum desired probability threshold
λ	Normalized tool life
$\boldsymbol{\theta}_f$	MLP weights/biases array at iteration f
θ_s	MLP parameters (weight and biases)
τ_m	Feed axis motor transmission ratio
κ_t	Drill-bit cutting-lip taper angle
$a(\cdot)$	MLP activation function
c	Feed per tooth
$\boldsymbol{d}_f$	Vector of process disturbances of PF
f	Flank wear measurement index
h	Undeformed chip thickness
$\bar{\imath}_{cut}$	Feed axis cutting current
$\bar{\imath}_{meas}$	Measured feed axis current
$\bar{\imath}_{motion}$	Feed axis current absorption (no cut)
i	Index for the hole number
$\tilde{k}_{c,a}$	Current axial cutting pressure
$\tilde{k}_{cs,a}$	Current axial specific cutting pressure
$k_{c,a}$	Axial cutting pressure
$k_{cs,t}$	Tangential specific cutting pressure
$k_{c,t}$	Tangential cutting pressure
K_m	Feed axis motor constant
n	Spindle speed
n_f	Noise of PF measurements
n_p	PF number of particles
$\bar{P}_{cut}$	Spindle cutting power
$\bar{P}_{meas}$	Measured spindle power
$\bar{P}_{motion}$	Spindle power absorption (no cut)
p	PF particle (i.e., MLP)
Q	Disturbances intensity
R	Noise variance
RUL_f	RUL PDF estimation at iteration f
$RUL_{p,f}$	RUL estimated at iteration f by particle p
RUL_{true}	True RUL of a specific drill-bit
r	Drill-bit radius
s	MLP parameter index
u	MLP activation function generic input
VB	Cutting edge flank wear measurement
VB_m	Drill-bit cutting edges' flank wear mean
v_c	Cutting speed
v_f	Feed speed

2.1. Inspection phase

The direct inspection of the drill-bit starts with flank pictures, each following four automatic pre-processing steps to centre images on the drill-bit flank (pre-processing 1, Fig. 2):

1. A grayscale transformation of the image is performed to reduce the image feature space [17].
2. Binarization with 120 as intensity threshold is performed to highlight the cutting edge.
3. The image is centred on the centre of mass of the masked area.
4. The image is cropped at a resolution of 900x400 pixels.

Five pre-processing steps follow (pre-processing 2, Fig. 2) to align reference drill-bit edges among different images:

5. Gaussian image blurring: an 11x11 Gaussian kernel is applied to smooth image noise.

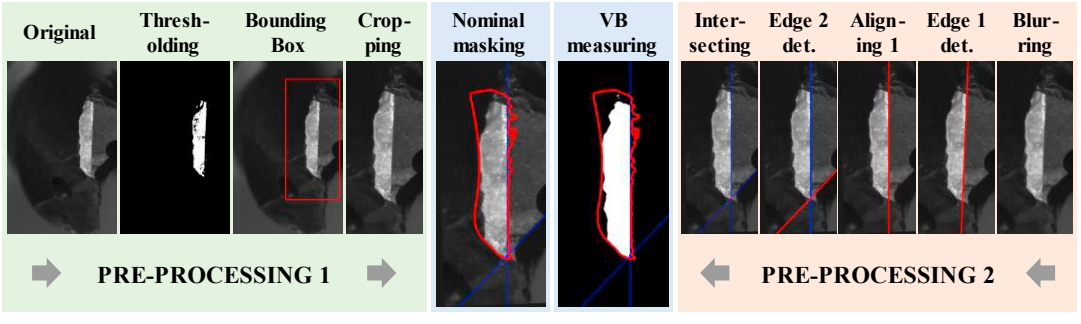

Fig. 2. Inspection phase workflow.

6. Detecting edge 1: a 2D convolutional filter highlights the vertical reference edge (in particular, edge 1).
7. Alignment 1: all the images are rotated to keep edge 1 vertical.
8. Detecting edge 2: a 2D convolutional filter is applied to the blurred image, followed by an Otsu's binarization [18] to highlight the oblique reference edge (edge 2).
9. Intersecting edges: intersection of the two edges is computed and becomes the reference point for the placement of the nominal cutting tool flank mask.

At last, the mean flank wear is computed. The worn drill-bit flank is masked through a binarization with 70 as intensity threshold (within nominal mask bounds). The difference between the nominal area and the highlighted area, divided by the flank length is the mean flank wear (VB) measurement of the cutting edge for that image. Since the drill-bit is made of two cutting edges, the flank wear measure is computed as the mean of the two at each stop, and it is indicated as VB_m. Kernels of the pre-processing filters presented above are reported in Table 1.

Table 1. Convolutional layers' kernels.

Layer	Edge 1 detection	Edge 2 detection
Kernel	$\begin{bmatrix} -4 & 0 & 4.5 \\ -4 & 0 & 4.5 \\ -4 & 0 & 4.5 \end{bmatrix}$	$\begin{bmatrix} -1.5 & \dots & -1.5 \\ 0 & \dots & 0 \\ 1.8 & \dots & 1.8 \end{bmatrix}$ $[3x20]$

2.2. Prognostics phase

Prognostics goal is to predict RUL of drill-bits. Prognostics phase forecasts the evolution of the mean flank wear VB_m and estimates the time at which it will overcome a preselected threshold. Two main features characterize the conceived prognostic approach: adaptivity to cutting parameters, i.e., the solution should be capable to predict RUL in an adaptive fashion starting from a limited set of training data in fixed working conditions (here, a single RTF is used); prediction of the RUL PDF, required by international standards but generally not provided by state-of-art approaches. Indeed, in this paper, a hybrid prognosis framework is conceived, similarly to crack growth propagation and Li-ion batteries prognosis [15], [16]. The solution consists in the integration of MLP (universal curve fitter) to fit flank wear degradation curves, and PF, to provide a Bayesian adaptive online training of multiple MLPs.

2.2.1. Multi-layer perceptron

MLP represents a naïve neural network, mapping between the input features and the outputs. In our problem, MLP maps VB_m as a function of the hole number i. Thus, the MLP has one input neuron and a single output neuron. To limit the MLP complexity, we introduce a single hidden layer with three neurons. The resulting MLP structure is shown in Fig. 3. The resulting MLP equation is presented in the following (Eq. (1)):

$$VB_m(i) = \theta_{10} + \sum_{s=1}^{3} \theta_{s+6}\, a(\theta_s\, i + \theta_{s+3}) \tag{1}$$

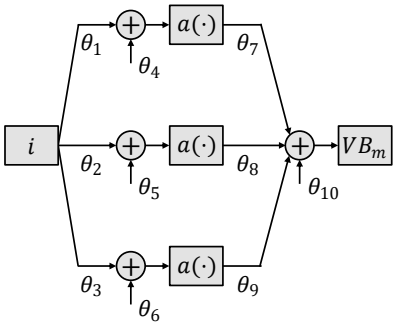

Fig. 3. Adopted multi-layer perceptron architecture.

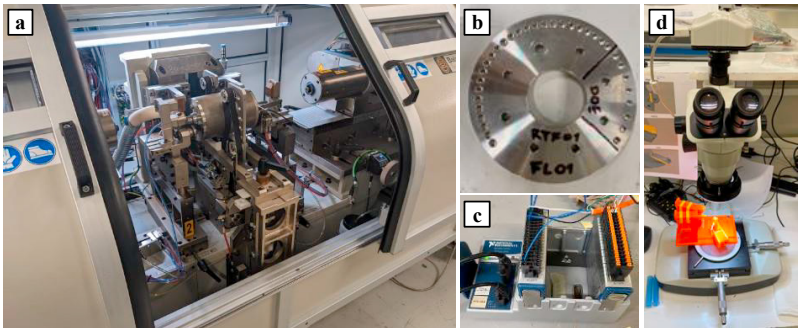

Fig. 4. Experimental set-up: a) balancing machine RB50A; b) workpiece flange; c) measurement set-up and DAQ; d) Optika SZN-T microscope.

where θ_1, θ_2, θ_3, θ_7, θ_8, θ_9 and θ_4, θ_5, θ_6, θ_{10} are the weights and biases of the MLP, respectively; $a(\cdot)$ is the activation function, defined by Eq. (2):

$$a(u) = u/(1 + |u|) \tag{2}$$

where u is a generic input. Thus, given the hole number i as input, the MLP returns the correspondent predicted flank wear $VB_m(i)$. The MLP is trained upon a single RTF test.

2.2.2. Particle filter

PF is an evolution of Kalman filter dealing with non-linear dynamical systems and non-gaussian measurement noise and process disturbances. PF approximates the dynamical system state PDF through a set of n_p particles (here, $n_p = 250$). In the developed solution, PF represents a mean to update the MLP fitting of VB_m, whenever a flank wear measurement becomes available. Moreover, a flank wear image is assumed available every 5 holes (we will call the associated index f, with $f = 0{,}5{,}10, \ldots$). Therefore, PF updates the MLP with 5 holes as sampling frequency. The developed PF observes the following dynamical system (Eq. (3)):

$$\begin{cases} \boldsymbol{\theta}_{f+1} = \boldsymbol{\theta}_f + \boldsymbol{d}_f \\ VB_{m,f}(i) = \theta_{10,f} + \sum_{s=1}^{3} \theta_{s+6,f}\, a\left(\theta_{s,f}\, i + \theta_{s+3,f}\right) + n_f \end{cases} \tag{3}$$

where $\boldsymbol{\theta}_f$ is the state of the dynamical system containing weights and biases of the MLP observed at hole f; $\boldsymbol{d}_f$ represents the process disturbances, assumed gaussian with null mean and diagonal covariance, proportional to $\boldsymbol{\theta}_f$ through disturbance intensity Q (here, $Q = 0.1$). The first equation is called *process equation* and it explores the weights and biases space at each PF iteration. The second equation is the *measurement equation*, and it provides the estimation of the measured quantity (i.e., VB_m) with the updated MLP. n_f is the measurement noise, assumed gaussian with null mean and standard deviation R (here, $R = 30$).

At each PF cycle a set of particles is sampled through the process equation. Thus, each particle p corresponds to a different state value, ending up in a different MLP. Resampling is the second PF step, which selects the most representative particles. Selection is performed by assigning a weight to each particle, proportional to the measurement likelihood (see [15], [16] for a detailed description of the resampling stage).

In order to perform prognostics, at each PF iteration, each resampled MLP (p) is evaluated to find the hole number corresponding to the threshold intersection (here, 150 μm). The correspondent hole number is $RUL_{p,f}$. RUL PDF (RUL_f) estimated at the f-th PF iteration is thus approximated through $RUL_{p,f}$, with $p = 1, \ldots, n_p$. In order to evaluate the performances of the conceived prognostics solution, two prognostic metrics were computed: absolute prediction error (APE) and prognostics horizon (PH), computed through the $\alpha - \beta$ criterion, with $\alpha = 0.20$ and $\beta = 0.95$ [19]. APE is computed as a function of the normalized tool life λ (Eq. (4)):

$$APE(\lambda) = \left|RUL_{true} - E[RUL_f]\right| \tag{4}$$

where $\lambda = f/RUL_{true}$; RUL_{true} is the actual hole number at which the flank wear overcame the threshold; $E\left[RUL_f\right]$ is the expected value of the estimated RUL PDF at the PF iteration f. PH is a measure of how long in advance the algorithm correctly predicts the RUL. Details on PH computation can be found in [19].

2.3. Experimental set-up and campaign

2.3.1. Set-up

The experimental set-up is composed of a CNC balancing machine RB50A from Balance Systems S.r.l. company (Fig. 4a). The experimental campaigns are performed on AISI303 stainless steel (Fig. 4b) using a drill-bit with 5.5 mm diameter and a cutting-lip taper angle κ_t of 70°. For the characterization of drill-bit wear during the RTFs, an Optika SZN-T microscope was used (Fig. 4d), with the help of a 3D-printed support for drill-bit positioning. In an industrial application scenario, the microscope can be substituted with cameras featuring macro lenses. Furthermore, a

supplementary acquisition system was installed to characterize the cutting process in the considered cutting parameters. The acquisition system consisted of an external DAQ from National Instruments (NI) DAQ9174 and two NI acquisition boards NI9205, to acquire a set of five analog and digital signals (Fig. 4c): machining/approaching (digital); feed speed, feed current, spindle speed and spindle power (analog). All the measured quantities were acquired at a sampling frequency of 1 kHz. In order to characterize the cutting process in the tested conditions, power and current measurements from the machine are firstly averaged on the stationary sections of a hole, and then non-cutting contributions ($\bar{P}_{motion}$ and $\bar{\imath}_{motion}$) removed, in order to obtain $\bar{P}_{cut}$ and $\bar{\imath}_{cut}$, respectively.

Then, specific cutting pressures are extracted from the two quantities (Eq. (5)):

$$\begin{aligned} k_{c,t} &= \bar{P}_{cut}/MRR \\ \tilde{k}_{c,a} &= k_{c,a}/(\tau_m K_m) = \bar{\imath}_{cut}/(2cr) \end{aligned} \tag{5}$$

where $k_{c,t}$ and $k_{c,a}$ are the tangential and axial cutting pressures; MRR is the material removal rate of the drilling operation; τ_m is the feed axis motor transmission ratio; K_m is the feed axis motor constant; c is the feed per tooth and r is the drill-bit radius. Since the motor transmission ratio and constant were unknown, only $\tilde{k}_{c,a}$ was estimated (proportional to the axial cutting pressure). Kronenberg's cutting pressures exponential models [20] are then derived from cutting pressures estimated by Eq. (5), through Eq. (6):

$$\begin{aligned} k_{c,t} &= k_{cs,t} h^{-x_t} \\ \tilde{k}_{c,a} &= \tilde{k}_{cs,a} h^{-x_a} \end{aligned} \tag{6}$$

where $k_{cs,t}$ and x_t, and $\tilde{k}_{cs,a}$ and x_a, are the specific cutting pressures in the tangential and axial direction, depending on the workpiece material-cutting tool pair; h is the chip thickness, equal to $c\sin(\kappa_t)$, where κ_t is the drill-bit cutting-lip taper angle.

2.3.2. Campaign

The experimentation consisted of two phases: experiments to characterize the cutting process and RTFs to develop and test drill-bit prognosis. Each hole consisted of 5 pecks, accounting for a total of 6 mm hole depth, in dry conditions. For the two experiment phases, a full-factorial design of experiments (DoE) with central point and validations was performed. The parameters of the DoE for the characterization phase, consisting of 25 cutting tests, were reported in Table 2, while the DoE parameters for the 12 RTFs were reported in Table 3. The test order was randomized.

3. Results and discussion

In this section, the results are reported following the order of the previously discussed experimental campaigns. The characterization of the cutting process is firstly presented through the estimation of specific cutting pressures. Secondly, inspection and prognosis results are discussed with regards to the RTF experimentation.

Table 2. DoE for cutting process characterization.

ID	c [level]	v_c [level]	c $[mm/tooth]$	v_c $[m/min]$	v_f $[mm/s]$	n $[rpm]$	Replicas
1	Low	Low	0.020	52	2.0	3000	4
2	Low	High	0.020	70	2.7	4051	4
3	High	Low	0.040	52	4.0	3000	4
4	High	High	0.040	70	5.4	4051	4
5	Mid	Mid	0.030	61	3.5	3526	5
6	Val	Val	0.035	66	4.4	3788	2
7	Mid	Low	0.030	52	3.0	3000	2

Table 3. DoE for run-to-failure tests.

ID	c [level]	v_c [level]	c $[mm/tooth]$	v_c $[m/min]$	v_f $[mm/s]$	n $[rpm]$	Replicas
1	Low	Low	0.020	52	2.0	3000	2
2	Low	High	0.020	70	2.7	4051	2
3	High	Low	0.040	52	4.0	3000	2
4	High	High	0.040	70	5.4	4051	2
5	Mid	Mid	0.030	61	3.5	3526	2
6	Mid	Low	0.030	52	3.0	3000	2

3.1. Cutting process characterization

This experimental campaign had the goal to check the cutting parameters adequacy for the drill-bit and workpiece material pair. Cutting pressures $k_{c,t}$ and $\tilde{k}_{c,a}$ trends, with respect to the undeformed chip thickness h were shown in Fig. 5. $\tilde{k}_{c,a}$ and $k_{c,t}$ trends were modelled through exponentials [20]. Model fits were good and described the behaviour of the two cutting pressures as a function of chip thickness h (with R-squared coefficients of 0.78 and 0.80, respectively). Simultaneous curve bounds (not including new observation variability) were reported, too. The observations fell inside the confidence bounds, including most of the validation data. The estimated model coefficients were $\tilde{k}_{cs,a} = 0.42\ A_{rms}/mm^2$, $x_a = 0.41$, $k_{cs,t} = 1933\ MPa$ and $x_t = 0.30$. The obtained values for tangential cutting pressures were usual for austenitic stainless steels, confirming a proper execution of the cutting process.

3.2. Run-to-failures

As explained in section 2.3, 12 RTFs were performed with different combinations of cutting speeds and feed per tooths. Direct inspection phase was applied to the RTFs. The wear progression during a sample RTF (test 1 (1)) was shown in Fig. 8, while the evolutions of the flank wears (i.e., the results of the application of the direct inspection phase) were shown in Fig. 7. The associated true End-of-Life of each test was reported in Table 4. Fig. 7 also demonstrates how the cutting speed and feed rate influence the flank wear evolution of the drill-bits. These relations were well known and higher cutting speeds, as well as higher feed rates, increase the wear rate of the drill-bit. However, the variability of degradation rates was high, even when the same parameters were used (same colours). This is the main reason why prognosis gained attention in the industrial scenario. Prognosis phase must face such variability in the flank wear evolutions and manage the effects of cutting parameters on tool wear rates, too. In order to predict the evolution of flank wear of drill-bits, prognostics was implemented. The algorithm was trained on one RTF (test 5 (1)) and tested on all the others, in order to show the adaptivity feature of the conceived solution. Prognostics results were shown in Fig. 6. This figure represents the trend of the estimated RUL over the normalized tool life λ. Image with label RTF 5 (1), represented the case where the algorithm was tested on the training RTF. It is important to track how the predicted RUL mean (blue solid line) and RUL 95% confidence intervals (RUL CIs, blue dashed lines) were positioned with respect to the true RUL (red solid line) and the acceptability region (red dashed

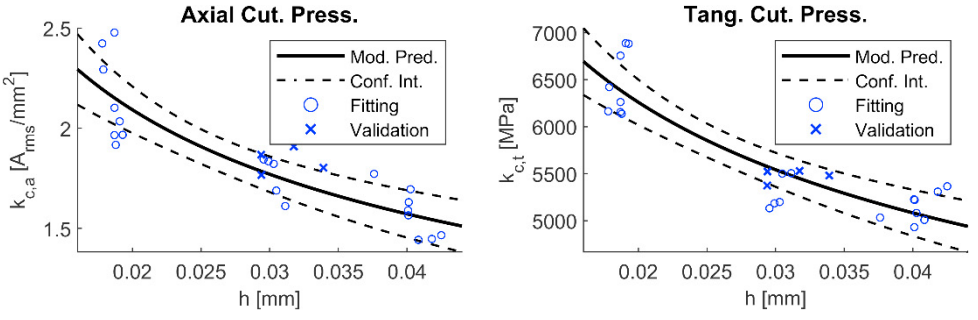

Fig. 5. Tangential and axial cutting pressure exponential model fitting.

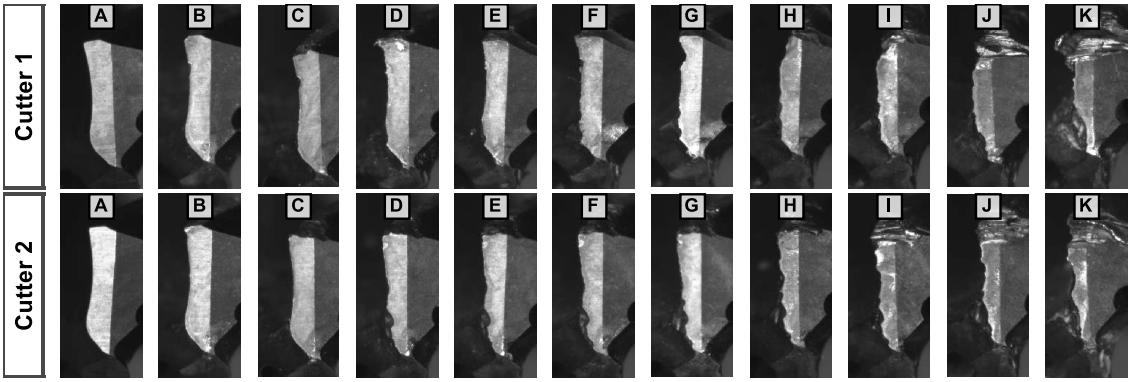

Fig. 8. RTF 1 (1) drill-bit cutters flank wear images.

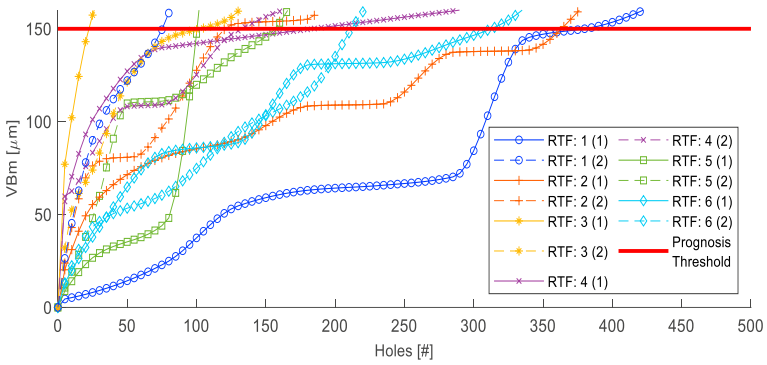

Fig. 7. Mean flank wear VB_m evolution during the 12 run-to-failures.

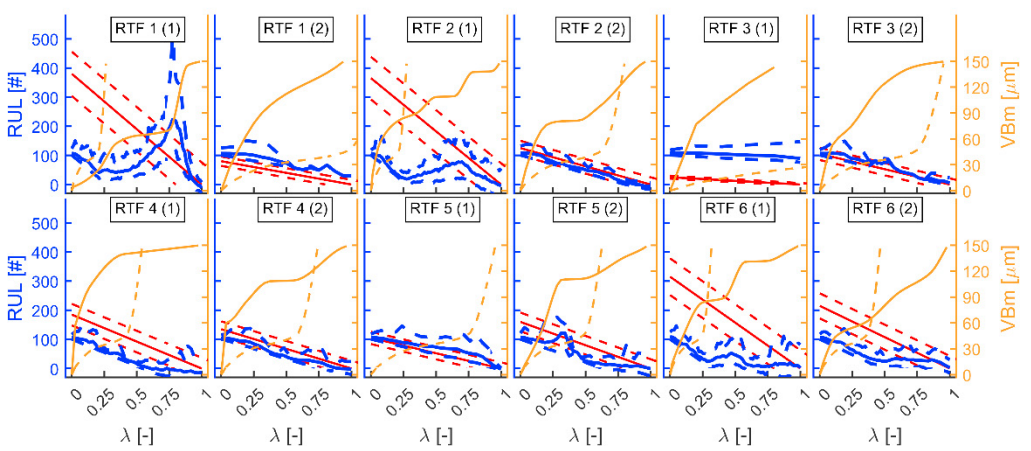

Fig. 6. Prognosis results when training is performed on test 5 (1).

Table 4. True End-of-Life (EoL) and prognosis horizon (PH) of the 12 drill-bits used in run-to-failures.

Test	1 (1)	1 (2)	2 (1)	2 (2)	3 (1)	3 (2)	4 (1)	4 (2)	5 (1)	5 (2)	6 (1)	6 (2)
EoL	381	77	365	122	24	104	185	134	102	158	314	213
PH [%]	11	0	22	100	0	14	0	19	10	9	2	26

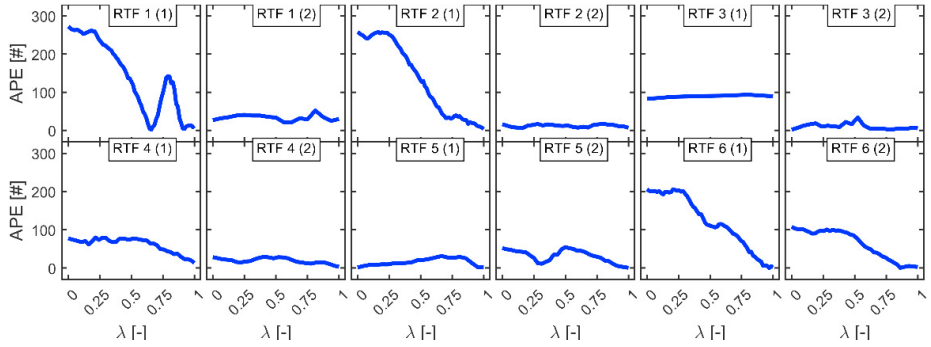

Fig. 9. Prognosis absolute prediction error when training is performed on test 5 (1).

lines) [19]. RUL CIs included the true RUL, and the RUL mean was included in the acceptability regions for most of the RTF execution. In Fig. 9, the associated APE was shown, which was almost constant and close to 0.

More attention should be given to the unseen cutting tests and parameters. The analysis should also consider that the results refer to a first application of the prognosis algorithm (only one run-to-failure available for training). New cutting tests, which become available from the field, should be included in the algorithm training. In each graph, the evolutions of VB_m of training and test RTFs were shown in orange, to graphically compare the curves. Test 1 (1) showed the maximum difference between the two. All the tests shown in Fig. 6, converged to the correct RUL, except for test 1 (2) and 3 (1). The APE for those tests were almost constant and around 30 and 100 holes respectively (Fig. 9). Indeed, a lack of adaptivity was detected only for these two RTFs. Correspondingly, in Table 4, the PH for these two tests was null, highlighting that RUL could not be predicted in advance. All the other tests faced converging RUL predictions or constant limited APEs. Table 4 reported that almost all the PHs were over the 10% of tool lives, meaning that the RUL could be robustly predicted in advance with a minimum of 10% leading time (i.e., allowing for their proper substitution). It must be noted that the PH was expressed as the last hole where the 95% of the estimated RUL PDF was included in the acceptability region (i.e., a restrictive condition), indicating that the confidence on a correct prediction was extremely high. Thus, PH were tendentially low (test 4 (1) faced a null PH, too), despite the errors in the prediction mean were limited in general (Fig. 9), with particular reference to RTFs 2 (1), 3 (2), 4(2) and 6 (1). This was not related to specific cutting conditions, but on the restrictive choice of β for the PH computation. Fig. 6 and Fig. 9 highlighted the algorithm reliability and stability (i.e., predictions gradually converge to the ground truth).

4. Conclusions

In this paper, a prognosis strategy was developed for drill-bits. Directly inspected flank wears were the inputs for a hybrid adaptive prognosis solution. The main advantages of the proposed solution were summarised in the following:

- Direct inspection allowed to automatically measure mean flank wear of a drill-bit starting from pictures of drill-bit cutting edges' flanks.
- Since in industrial scenarios cutting edge pictures are available only at pit-stops, prognosis was updated every 5 holes, forecasting the flank wear evolution of the drill-bit adaptively.
- Prognosis gave estimates of the RUL probability density function online, providing a tool to statistically support the maintenance decision making.
- Adaptivity of the conceived approach allowed to predict drill-bit wear evolution under unseen process parameters, using just one training run-to-failure (with 7 out of 12 RTFs predicted with a prognosis horizon greater than 10% and only three RTFs with a null prognosis horizon). This allows its implementation when worn data are scarce (small batch production or one-of-a-kind production).
- The algorithm performances were compared with respect to the original separated components (i.e., MLP and PF). The hybrid solution outperformed both the algorithms: PF scored three 21% prognostics horizons and nine null ones; MLP scored three prognostics horizons of 100% and nine null ones.

Future works will consist in the development of a heterogeneous prognosis approach, where specific cutting pressures will be included in the prediction of flank wear, providing a cutting parameter independent feature, to update the RUL predictions even when a pit-stop is not an option.

Acknowledgements

Authors would like to thank Balance Systems' staff for their collaboration. This research was developed within the Humans Hub project, funded by "Asse Prioritario I – Azione I.1.b.1.3 POR-FESR 2014 – 2020 Regione Lombardia" and a PhD grant (ID27 - "Prognostics and Health Management in Machine Tool and Manufacturing Industry") in DGR 769-2018 funded by Emilia-Romagna region.

References

[1] X. Xu, Y. Lu, B. Vogel-Heuser, e L. Wang, «Industry 4.0 and Industry 5.0—Inception, conception and perception», *Journal of Manufacturing Systems*, vol. 61, pp. 530–535, ott. 2021, doi: 10.1016/j.jmsy.2021.10.006.

[2] X. Zhang, S. Wang, W. Li, e X. Lu, «Heterogeneous sensors-based feature optimisation and deep learning for tool wear prediction», *International Journal of Advanced Manufacturing Technology*, vol. 114, fasc. 9–10, pp. 2651–2675, giu. 2021, doi: 10.1007/S00170-021-07021-6/FIGURES/22.

[3] P. Stavropoulos, A. Papacharalampopoulos, E. Vasiliadis, e G. Chryssolouris, «Tool wear predictability estimation in milling based on multi-sensorial data», *International Journal of Advanced Manufacturing Technology*, vol. 82, fasc. 1–4, pp. 509–521, 2016, doi: 10.1007/s00170-015-7317-6.

[4] A. Rizzo *et al.*, «The Critical Raw Materials in Cutting Tools for Machining Applications: A Review», *Materials*, vol. 13, fasc. 6, p. 1377, mar. 2020, doi: 10.3390/ma13061377.

[5] B. Guo, Q. Zhang, Q. Peng, J. Zhuang, F. Wu, e Q. Zhang, «Tool health monitoring and prediction via attention-based encoder-decoder with a multi-step mechanism», *Int J Adv Manuf Technol*, ago. 2022, doi: 10.1007/s00170-022-09894-7.

[6] B. Yan, L. Zhu, e Y. Dun, «Tool wear monitoring of TC4 titanium alloy milling process based on multi-channel signal and time-dependent properties by using deep learning», *Journal of Manufacturing Systems*, vol. 61, pp. 495–508, ott. 2021, doi: 10.1016/j.jmsy.2021.09.017.

[7] J. Yu, S. Liang, D. Tang, e H. Liu, «A weighted hidden Markov model approach for continuous-state tool wear monitoring and tool life prediction», *The International Journal of Advanced Manufacturing Technology*, vol. 91, fasc. 1, pp. 201–211, 2017, doi: 10.1007/s00170-016-9711-0.

[8] M. Nouri, B. K. Fussell, B. L. Ziniti, e E. Linder, «Real-time tool wear monitoring in milling using a cutting condition independent method», *International Journal of Machine Tools and Manufacture*, vol. 89, pp. 1–13, 2015, doi: 10.1016/j.ijmachtools.2014.10.011.

[9] D. Shi e N. N. Gindy, «Tool wear predictive model based on least squares support vector machines», *Mechanical Systems and Signal Processing*, vol. 21, fasc. 4, pp. 1799–1814, mag. 2007, doi: 10.1016/j.ymssp.2006.07.016.

[10] C. Drouillet, J. Karandikar, C. Nath, A.-C. Journeaux, M. El Mansori, e T. Kurfess, «Tool life predictions in milling using spindle power with the neural network technique», *Journal of Manufacturing Processes*, vol. 22, pp. 161–168, apr. 2016, doi: 10.1016/j.jmapro.2016.03.010.

[11] A. Jiménez, M. Arizmendi, e J. M. Sánchez, «Extraction of tool wear indicators in peck-drilling of Inconel 718», *International Journal of Advanced Manufacturing Technology*, vol. 114, fasc. 9–10, pp. 2711–2720, giu. 2021, doi: 10.1007/S00170-021-07058-7/TABLES/4.

[12] Y. Peng, M. Dong, e M. J. Zuo, «Current status of machine prognostics in condition-based maintenance: A review», *International Journal of Advanced Manufacturing Technology*, vol. 50, fasc. 1–4, pp. 297–313, 2010, doi: 10.1007/s00170-009-2482-0.

[13] O. Moldovan, S. Dzitac, I. Moga, T. Vesselenyi, e I. Dzitac, «Tool-Wear Analysis Using Image Processing of the Tool Flank», *Symmetry*, vol. 9, fasc. 12, p. 296, nov. 2017, doi: 10.3390/sym9120296.

[14] L. Fernández-Robles, L. Sánchez-González, J. Díez-González, M. Castejón-Limas, e H. Pérez, «Use of image processing to monitor tool wear in micro milling», *Neurocomputing*, vol. 452, pp. 333–340, set. 2021, doi: 10.1016/j.neucom.2019.12.146.

[15] F. Cadini, C. Sbarufatti, M. Corbetta, F. Cancelliere, e M. Giglio, «Particle filtering-based adaptive training of neural networks for real-time structural damage diagnosis and prognosis», *Structural Control and Health Monitoring*, vol. 26, fasc. 12, pp. 1–19, 2019, doi: 10.1002/stc.2451.

[16] C. Sbarufatti, M. Corbetta, M. Giglio, e F. Cadini, «Adaptive prognosis of lithium-ion batteries based on the combination of particle filters and radial basis function neural networks», *Journal of Power Sources*, vol. 344, pp. 128–140, 2017, doi: 10.1016/j.jpowsour.2017.01.105.

[17] N. Carbone, L. Bernini, P. Albertelli, e M. Monno, «Assessment of milling condition by image processing of the produced surfaces», *Int J Adv Manuf Technol*, vol. 124, fasc. 5–6, pp. 1681–1697, gen. 2023, doi: 10.1007/s00170-022-10516-5.

[18] N. Otsu, «A Threshold Selection Method from Gray-Level Histograms», *IEEE Trans. Syst., Man, Cybern.*, vol. 9, fasc. 1, pp. 62–66, gen. 1979, doi: 10.1109/TSMC.1979.4310076.

[19] A. Saxena, J. Celaya, B. Saha, S. Saha, e K. Goebel, «Metrics for offline evaluation of prognostic performance», *International Journal of Prognostics and Health Management*, vol. 1, fasc. 1, pp. 2153–2648, 2010, doi: 10.36001/ijphm.2010.v1i1.1336.

[20] M. Kronenberg, *Machining Science and Application, Theory and Practice for Operation and Development of Machining Processes*. Oxford: Pergamon Press, 1966.